

The Integration of 3D Carbon-electrode Dielectrophoresis on a CD-like Centrifugal Microfluidic Platform

Rodrigo Martinez-Duarte,*^a Robert A. Gorkin III,^b Kameel Abi-Samra^b and Marc J. Madou^{a,b}

Received (in XXX, XXX) Xth XXXXXXXXX 200X, Accepted Xth XXXXXXXXX 200X

5 First published on the web Xth XXXXXXXXX 200X

DOI: 10.1039/b000000x

We introduce the integration of a novel dielectrophoresis (DEP)-assisted filter with a compact disk (CD)-based centrifugal platform. Carbon-electrode dielectrophoresis (carbon-DEP) refers to the use of carbon electrodes to induce DEP. In this work, 3D carbon electrodes are fabricated using the C-MEMS technique and are used to implement a DEP-enabled active filter to trap particles of interest. Compared to traditional planar metal electrodes, 3D carbon electrodes allow for superior filtering efficiency. The system includes mounting modular 3D carbon-DEP chips on an electrically-interfaced rotating disk. This allows simple centrifugal pumping to replace the large footprint syringe pump approaches commonly used in DEP systems. The advantages of the CD setup include not only a reduced footprint, but also complexity and cost reduction by eliminating expensive precision pumps and fluidic interconnects. To demonstrate the viability of this system we quantified the filter efficiency in the DEP trapping of yeast cells from a mix of latex and yeast cells. Results demonstrate selective filtering at flow rates up to 35 $\mu\text{L min}^{-1}$. The impact of electrode height, DEP chip misalignment and particle sedimentation on filter efficiency and the advantages this system represents are analyzed. The ultimate goal is to obtain an automated platform for bioparticle separation with application in different fields such as point-of-care diagnostics and cell-based therapies.

Introduction

Lab-on-a-chip (LOC) refers to the integration of different laboratory processing steps into a monolithic device. These processes can include sample preparation, purification, sorting, amplification and signal detection. Different capabilities must be incorporated onto the monolithic device to allow for the manipulation of fluid and/or targeted entities and for the sensing and detection of relevant phenomena. In this work we employed centrifugal forces for the manipulation of the fluid and carbon electrodes for the selective trapping of targeted particles. Advantages of LOC devices include their small size, low sample volume requirements, rapid analysis and the fact that a LOC device eliminates the intervention of skilled personnel to perform a clinical assay. LOC-based platforms like the one introduced here are expected to effectively minimize the footprint, complexity and cost of clinical diagnostics and other health care-related platforms to enable the replacement of centralized, expensive laboratories by point-of-care, portable instruments. LOC-based instruments can improve global health dramatically, especially in developing countries where the lack of medical infrastructure is one of the main causes of high mortality rates¹. Unfortunately, even though the potential of LOC-based platforms in a variety of applications is clear²⁻⁶, only a few commercial systems have been demonstrated in the field, for example the i-STAT[®] portable clinical analyzer by Abbott Point of Care, Inc.⁷ and the Piccolo[®] xpress from Abaxis, Inc.⁸

50 Here we present the integration of a 3D carbon-electrode dielectrophoresis (carbon-DEP) filter on a Compact Disk

(CD)-like centrifugal platform with the objective of developing an automated platform for bioparticle separation with application in point-of-care diagnostics and cell-based therapies.

Dielectrophoresis (DEP) enables the selective manipulation of a targeted particle, or population of particles, using the interaction of a non uniform electric field with the induced effective dipole moment of the particle(s)⁹. DEP is advantageous over other particle separation techniques such as FACS (Fluorescence-activated cell sorting) and MACS[®] (Magnetic-activated cell sorting) because discrimination between different particles is based solely on their intrinsic physical properties, *i. e.*, membrane morphology and internal compartmentalization in the case of cells, and not on external tags. These physical properties determine the particle's dielectric properties and give it a characteristic dielectric phenotype. DEP works best when the dielectric phenotype of the targeted particle(s) significantly differs from those of other particles present in the sample¹⁰. However, when operating in a flow system for continuous separation, populations with subtle differences can be separated by DEP but only at very low flow rates¹¹. In any case, the use of DEP eliminates functionalized magnetic beads or fluorophores required by other separation techniques such as magnetophoresis and flow cytometry. The elimination of these often expensive labels reduces assay complexity, time and costs which can expand the availability of diagnostic tests, such as for HIV, and make therapies for cancer or degenerative diseases available to a broader number of patients. For example, DEP was demonstrated in the purification of blood and bone marrow from cancer cells¹²⁻¹⁴

and in the enrichment of stem cell populations¹⁵⁻¹⁸. For further reading, an excellent review on DEP fundamentals and the use of DEP in diagnostics is by Gascoyne and Vykoukal¹⁹.

Even though assay costs are reduced with the elimination of labels, a millimeter-sized DEP chip must still be interfaced to large and often expensive precision apparatus for fluid dispensing. Traditional DEP platforms rely on a combination of syringes, tubing, valves, and fluidic ports for fluid manipulation that significantly increases their complexity and has prevented the implementation of DEP-based platforms in settings other than research. In this work we replaced the traditional syringe piston pumping by centrifugal pumping on an electrically-interfaced compact disk (CD)-like microfluidics platform. The use of a CD platform significantly reduces the footprint and cost of a DEP system and makes it amenable for assay automation. The entire fluid network is contained in a single DEP chip to eliminate the use of syringes, external valves, tubing and any other supporting fluidic elements. This work differs from DEP platforms where electroosmosis is used as pumping force in that centrifugal pumping does not depend on the electric nor physicochemical properties of the sample.

The proposed combination of centrifugal and electric forces in a single platform has been reported before. Wang and colleagues demonstrated a dual-pumping CD-like electrophoresis-based separation system where the centrifugal and electrophoresis forces in the CD are balanced to obtain a better separation of the dyes rhodamine B and xylene cyanole. This system differs from the one presented here in that only DC electrical signals were coupled to the rotating platform. An electrophoresis force is used to attract the most negatively charged dye towards the center of the CD while a centrifugal force pushes the heaviest dye (xylene cyanole) to the rim of the CD²⁰. Fuhr et al.^{21, 22} disclosed a swinging-rotor centrifugal system to conduct DEP with metal-electrodes using AC electrical signals. In contrast to our current CD-like rigid platform, the DEP devices in Fuhr et al's work are first aligned parallel to the center of rotation and gradually move to a position perpendicular to the rotation axis as the rotation speed increases (resembling a fairground carousel with swings). The use of a horizontal rigid platform such as the one demonstrated here yields a system with low height profile and, most importantly, eliminates moving parts (hinges for example) to add robustness to the platform. Another system somewhat similar to the one presented here is the one demonstrated by Boettcher et al²³. In their approach a metal-electrode based DEP chip, a PCB-mounted signal generator and a couple of 9V batteries are positioned on a rotating platform. The Boettcher et al system differs from ours in two important respects: 1) it does not have the capability for remote control so that the signal generator's frequency and amplitude must be set before the experiments, and 2) the throughput, as it uses 2D metal electrodes, is low.

Our goal is to implement an automated sample-to-answer system where human intervention is only needed to load a sample from a patient, e.g. blood, saliva or urine, choose the assay to be performed and retrieve either a numeric result, for example the number of CD4+ T-cells present in HIV patients,

or an enriched cell population to be used in cell therapy. Here we employ carbon-electrode dielectrophoresis (carbon-DEP) to demonstrate DEP on the CD platform. Carbon-DEP refers to the use of carbon electrodes to induce dielectrophoresis (more details in the Background section). The initial proof-of-concept of this platform was presented recently³⁹. In the current paper we clarify the fabrication process of the platform and demonstrate the selective filtering of yeast cells from a latex-yeast mixture using carbon-DEP. This work represents an important step towards the final goal of integrating all types of electrokinetic phenomena (AC and DC) to other functions we already demonstrated on CD platforms including valving, decanting, calibration, mixing, metering, sample splitting, and fluid separation.

Background

Compact disk (CD)-like centrifugal platform

Microfluidic CD technology has been developed as a unique alternative for handling biological analysis²⁴⁻²⁶. CD microfluidics rely on forces and pressure gradients induced on a spinning CD platform to move sample liquids. In its most basic form, fluids are propelled towards the outer radius of the disk by a centrifugally induced pressure gradient. Other forces present on spinning objects include Coriolis and Euler forces and may also be employed^ψ. The advantages of centrifugal pumping compared to other standard propulsion techniques such as syringe pumps, ultrasonic, or electrokinetic pumping have been well documented in Madou et al²⁴. Key benefits of centrifugal pumping described in the latter reference are its insensitivity to most physicochemical properties of the sample being pumped, such as pH, ionic strength or chemical composition, the fact that the system is easy to miniaturize and that it lends itself easily to assay multiplexing.

The envisioned benefits of CD microfluidics have motivated the continued steady development of this platform over the last 40 years. In this time span, a wide variety of fluidic functions including valving, decanting, mixing, etc. have been utilized to enable a variety of biological assays on "Lab-on-a-CD" setups (see Table 1). Examples of commercial applications of Lab-on-a-CD technology include the Piccolo[®] xpress (from Abaxis, Inc.⁸) for a blood electrolyte analysis and Gyrolab[®] (from Gyros AB²⁷) for the automation of immunoassay processing.

Carbon-electrode dielectrophoresis (carbon-DEP)

Glass-like carbon[§] electrodes are derived through the pyrolysis of photo patterned SU-8, a negative epoxy-based UV photoresist. Even though other DEP designs based on different materials can be used with the CD platform, the use of carbon electrodes yields some key benefits that make carbon-DEP an alternative to metal-electrode based DEP or insulator-based dielectrophoresis (iDEP).

The implementation of a dielectrophoresis force on a sample requires a non uniform electric field across the sample (details under Theory). This non uniform field creates volumes of different electric field magnitudes across the sample where

Table 1. Biological assays and fluidic functions performed using a Lab-on-a-CD setup

Biological assay	Fluidic function					References
	Valving	Decanting	Mixing	Metering	Sample Splitting	
Whole blood processing	X	X		X		8, 28-30*
Colormetric detection of biochemical markers	X		X	X	X	8, 29*
Sample lysis and homogenization	X	X		X		31
Nucleic acid amplification	X		X			32, 33
Immunoassay	X		X	X	X	27, 30, 34
DNA microarray hybridization	X				X	35-37
Cell culture and manipulation	X					23, 38, 39
Organism culture	X			X		40, 41

*Note: in the Abaxis system^{8, 29} both whole blood processing and colormetric detection of biochemical markers are integrated in one disk but their fluidic functions are isolated from each other. After blood processing the sample is transferred to a separate set of chambers where is split and mixed with reagents for colormetric detection

particles can be selectively positioned according to their dielectric phenotype and different experimental parameters. Most of the work in DEP relies on the use of metal microelectrodes contained in a flow channel to induce such non uniform electric field in the sample. However, the use of metal microelectrodes in direct contact with the sample severely restricts the magnitude of the applied voltages as one must prevent sample electrolysis. Moreover, the fabrication of metal electrodes, especially when dealing with 3D electrodes rather than planar (2D) electrodes, quickly turns relatively complicated and expensive. For example, the use of 3D metal electrodes (e.g., a set of high-aspect ratio posts) requires the use of metal electroplating that often restricts high yields and may result in more expensive devices. Examples of DEP work with electroplated gold structures are the works by Wang et al.⁶⁸, who incorporates the 3D electrodes in the side-walls of a microfluidic channel and uses DEP to focus a stream of particles, and by Voldman et al.⁶⁹, who implements a cell interrogation site for flow cytometry applications by using DEP to trap cells in between 3D electrodes. An alternative to the use of metal microelectrodes as detailed above is to use arrays of insulator structures, usually fabricated from polymers or glass, to locally distort the electrical field. In this technique, known as insulator-based dielectrophoresis or iDEP⁴²⁻⁴⁵, metal electrodes (for example extruded wire rods or machined metal plates) positioned outside the flow channel are used to set up the field over the insulator structures. A voltage as high as thousands of volts is applied to the metal electrodes to generate a uniform electric field that is rendered non uniform in the vicinity of the insulator structures. When using this technique, the sample is usually contained in the insulator array and the possibility of electrolyzing the sample is minimized. However, iDEP requires very high voltages (electric field magnitude is inversely proportional to the gap between electrodes and in iDEP the separation between metal electrodes can be in the order of centimeters) to create a suitable electric field for dielectrophoresis.

Carbon-DEP combines the advantages of metal-based and insulator-based DEP. For example, the possibility of sample electrolysis is reduced with the use of carbon electrodes, an advantage shared with iDEP, while low voltages are enough to polarize the carbon electrodes and create an electrical field

suitable for DEP, an advantage shared with metal-electrode DEP. The possibility of sample electrolysis is minimized when using carbon electrodes because carbon has a much wider electrochemical stability window than metals commonly used in thin film electrode fabrication such as gold and platinum and affords higher applied voltages in a given solution without electrolyzing it^{46, 46}. Even though the electrical conductivity of glass-like carbon^{47, 48} is lower than that of metals, suitable electric fields for DEP can be generated by polarizing carbon electrodes with voltages in the range of tens of volts instead of the hundreds or thousands of volts between metal plates required in iDEP. The use of carbon electrodes yields other advantages: 1) excellent biocompatibility^{49, 50}, 2) chemically very inert in almost all solvents/electrolytes^{51, 52} and 3) excellent mechanical properties^{53, 54}. Furthermore, carbon 3D electrodes can be fabricated using the Carbon MEMS (C-MEMS)[†] technique in a very simple high yield process^{46, 55}. In this work, the use of 3D structures that cover most of the height of a flow channel greatly improves filter throughput by reducing the mean distance of any particle to the closest electrode surface. This is in contrast to the filter throughput achieved when using 2D (planar) electrodes positioned at the bottom of a flow channel where many targeted particles immersed in the bulk volume of the channel do not come close to the electrical field gradient surrounding the planar electrodes and cannot get trapped (prior simulation work⁵⁶ of the DEP force induced by carbon electrodes shows a strong DEP effect close to the electrode surfaces that diminishes as one moves away from the electrodes into the bulk of the solution). The use of 3D electrodes reduces or eliminates the number of re-flow cycles that are required to improve filter throughput when using 2D electrodes. 3D carbon-DEP has been demonstrated for the discrimination of viable yeast cells from non viable ones, the filtration of yeast cells against a flow and the selective manipulation of latex particles⁵⁷⁻⁶¹. The improvement on filter efficiency when using 3D carbon electrodes instead of planar ones has already been quantified⁶². Modeling and simulation work has also been carried out^{48, 56, 60, 63}.

Theory

Centrifugal

The flow rate Q in a micro channel featuring laminar, viscous and incompressible flow is given by the general equation:

$$(1) \quad Q = \frac{\Delta P}{R}$$

where ΔP denotes a pressure gradient and R the fluidic resistance exhibited by the channel. This resistance depends on the cross section of the channel. For example, in the case of a circular cross section the Hagen-Poiseuille equation applies with $R = 128\mu L/\pi D^4$ where D is the diameter of the channel cross-section, L is the length of the channel and μ is the dynamic viscosity (in Ns m^{-2}). In the case of a rectangular cross section with an aspect ratio $\gg 1$, the fluidic resistance R is given by⁶⁴:

$$(2) \quad R = \frac{12\mu L}{wh^3}$$

where L is the length of the channel and w and h are the width and height of the channel cross-section respectively. The flow rate in a rectangular cross section micro channel is thus obtained as:

$$(3) \quad Q = \frac{\Delta P wh^3}{12\mu L}$$

The centrifugal pressure P_c depends on the distance r from the center of rotation as:

$$(4) \quad \frac{\delta P_c}{\delta r} = \rho \omega^2 r$$

where ρ is the density of the fluid and ω is the angular velocity of the centrifugal platform. Integration of Equation 4 from r_1 , the point of the channel closest to the center of the disc, to r_2 , the point of the channel furthest away from the center, results in:

$$(5) \quad \Delta P_c = \rho \omega^2 r \Delta r$$

Where $\bar{r} = (r_2 + r_1) / 2$ and $\Delta r = r_2 - r_1$. Plugging Equation 5 into Equation 3 thus yields the flow rate induced by the centrifugal force in a channel of rectangular cross section as:

$$(6) \quad Q = \frac{\rho \omega^2 r \Delta r wh^3}{12\mu L}$$

Dielectrophoresis

The dielectrophoresis force F_{DEP} on a spherical particle of

radius r in a medium m is given by:

$$(7) \quad F_{DEP} = 2\pi \epsilon_m r^3 \text{Re}[f_{CM}] |\nabla E_{rms}|^2$$

$$(8) \quad \text{with } \text{Re}[f_{CM}] = \frac{\epsilon_p^* - \epsilon_m^*}{\epsilon_p^* + 2\epsilon_m^*}$$

where r denotes the radius of the particle, $|\nabla E|$ the magnitude of the electric field gradient, ϵ_p^* the complex permittivity of the particle and ϵ_m^* of the media. Complex permittivity ϵ^* is given by:

$$(9) \quad \epsilon^* = \epsilon - \frac{j\sigma}{2\pi f}$$

and depends on the permittivity ϵ and conductivity σ of the particle or the media and the frequency f of the applied electric field. The imaginary number $\sqrt{-1}$ is represented by j . A non uniform electric field is necessary to induce a DEP force as stated in Equation 7 (otherwise $|\nabla E| = 0$). Positive values of $\text{Re}[f_{CM}]$, see Equation 8, for a given particle denote the induction of a DEP force that causes it to migrate towards regions of high electric field magnitude (positive DEP) while negative values of $\text{Re}[f_{CM}]$ denote the opposite behavior with particles moving towards regions of low or no electric field (negative DEP). The magnitude of the induced DEP force on a particle with fixed radius r is proportional to the absolute value of $\text{Re}[f_{CM}]$ and the magnitude of the electric field gradient squared. In the work presented here, positive DEP is induced on yeast cells, both viable and non viable, to extract them from a mixture of yeast cells and latex particles and trap them on the surface of the electrodes against the fluid flow (the positive DEP force must be stronger than the hydrodynamic drag force in this case). In contrast, a negative DEP force is induced on the latex particles to repel them from the electrode surface and facilitate their elution from the channel in the fluid flow.

Experimental setup

The experimental setup consists of five parts: 1) a programmable motorized spin stand, 2) a function generator, 3) a specialized spin chuck, 4) a compact disk (CD) platform and 5) carbon-DEP chips. Assembly of the system is illustrated in Fig. 1. The CD platform is mechanically connected to the motor through a custom-made spin chuck that features a slip ring arrangement needed to electrically connect the function generator to the spinning platform. An electrical network is contained on the CD platform to interface the signal coming from the function generator to the DEP chips. The DEP chips, incorporating both the DEP electrodes and the microfluidic network, are placed on the

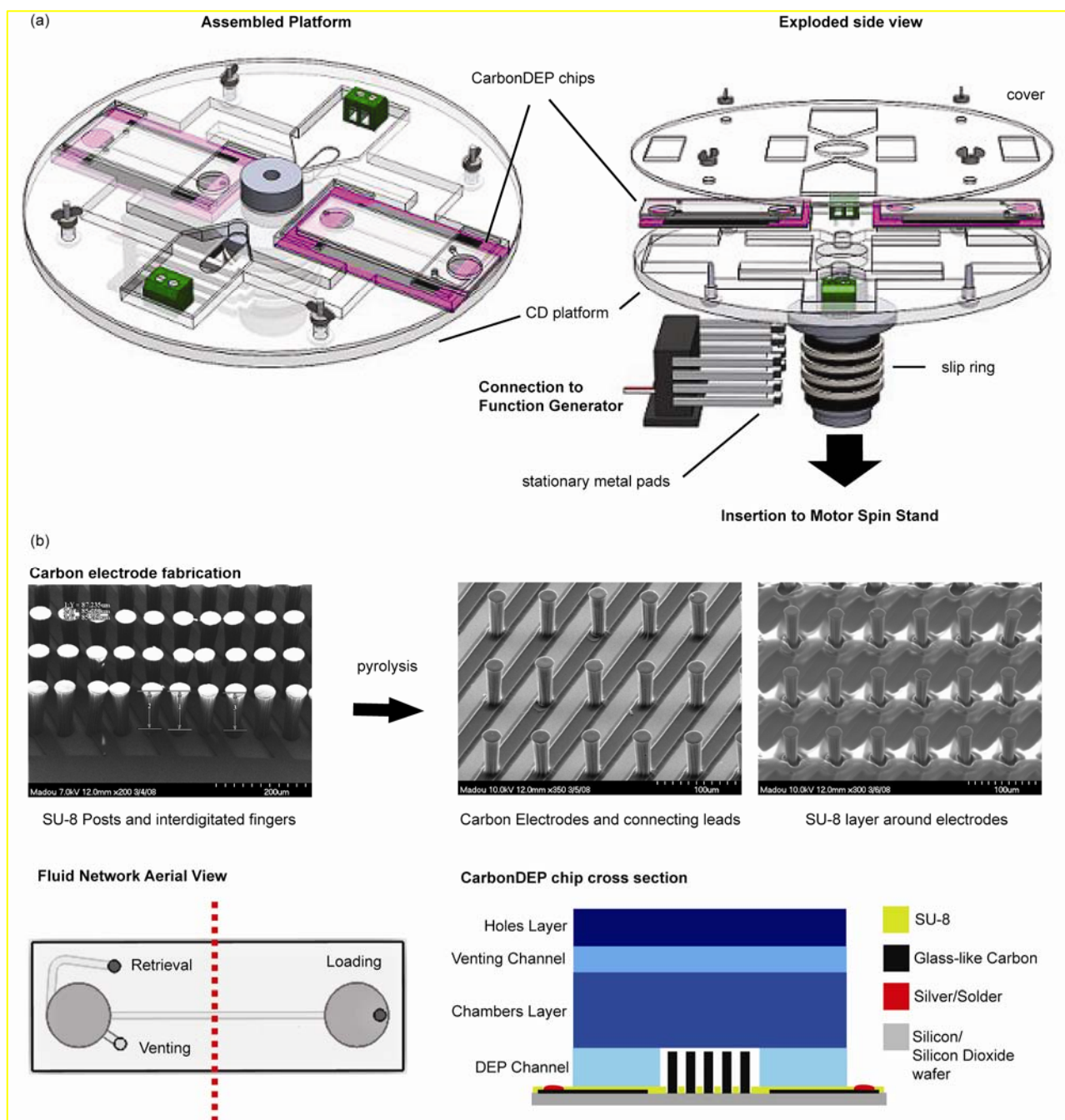


Figure 1 (a) Experimental setup and its assembly. (b) 3D carbon-DEP chip fabrication: (top) carbon electrodes are derived by the pyrolysis of photopatterned SU-8. Fluid network aerial view (bottom-left) and chip cross section at dotted line (bottom-right)

CD platform using designated slots. This modular arrangement makes for a user-friendly and rapid experimentation setup.

Motor spin stand

The spin stand consists of a motor (Pacific Scientific Servo Motor) and its amplifier/controller (PAC SCI Programmable Servo Drive). The motor drive utilizes a graphical user interface program, ToolPAC, to easily configure and program the motor for varying spin profiles. An imaging system was

utilized to examine fluid flow. The system is composed of a camera (Basler A301bc, 640 × 480 pixels, 80 fps max., 10× zoom lens mounted), a strobe light (PerkinElmer MVS-4200, 6 μs duration), and a retro-reflective fiber-optic sensor (Banner D10 Expert Fiber-Optic Sensor). To trigger the camera, a reflective marker is placed on the surface of the CD and aligned with the fiber-optic sensor. When the sensor detects the marker, a signal pulse is sent to the video capture board, triggering the camera and strobe light to acquire one image frame per CD revolution. This imaging system did not allow for the visualization of particles, averaging 8 μm in

diameter, and was only used to analyze fluid flow and determine flow rates in the micro channel.

Function generator

Sinusoidal voltage signals of different frequency and amplitude are generated by a Stanford Research Systems DS345 Function Generator. The specifications of this instrument include maximum working amplitude and frequency of 20 V_{pp} (peak-to-peak) and 20 MHz respectively.

Spin chuck and compact disk platform

A custom-made aluminum spin chuck mechanically interfaces the compact disk platform to the motorized spin stand and enables an electrical connection between the spinning platform and the function generator using a slip ring. A slip ring is a hollow ceramic cylinder featuring metal (silver in this case) rings on its outer surface that once inserted around the spin chuck yields a permanent contact between the silver rings and a set of stationary brushes (silver graphite in our case) while spinning the chuck and the CD platform. The stationary brushes are wired to the function generator and the electric signal from the function generator is delivered via the slip ring to the spinning CD platform where is guided to the DEP chips using miniature screw-clamp terminal blocks and simple wiring. The compact disk platform allows for modular deployment of DEP chips and features a bottom substrate and a top cover. The bottom substrate (2.54 mm thick polycarbonate) contains the DEP chips in designated compartments while the top cover (1 mm thick polycarbonate) is used to prevent the DEP chips from detaching from the platform while spinning. Stainless steel nuts and bolts are used for the alignment of top cover to the bottom substrate and to secure the two polycarbonate pieces together. The platform used in this work can hold two carbon-DEP chips. The resulting platform, we call SpinDEP, features programmable centrifugal pumping and electrical forces.

3D Carbon-electrode dielectrophoresis chips

3D carbon-DEP chips are fabricated as stand-alone units, or modules, to allow for a rapid insertion and removal to and from the CD platform. Carbon-DEP chips feature 3D carbon electrodes that are obtained by the pyrolysis, or thermal degradation, of organic polymer precursor structures using the C-MEMS technique⁴⁶. SU-8 (MicroChem, Newton, MA), a UV epoxy-based negative photoresist, is used as the polymer precursor for carbonization. The fabrication process is summarized in Fig. 1 (b). Briefly, the process starts with a two-step photolithography process to fabricate the precursor SU-8 structures. Pyrolysis, heating of the precursor structures to 900 °C in an inert atmosphere, is then used to convert the polymer structures into the 3D carbon electrodes (two different heights of carbon electrodes are used in this work: 40 and 70 μm) and their connecting electrical leads. A thin SU-8 layer is patterned around the 3D electrodes and is used to protect the connecting leads from contact with the solution.

The fluid network required for the DEP chip is fabricated using polycarbonate (PC) and double-sided pressure-sensitive adhesive and features two channels. The main flow channel is 600 μm wide by 100 μm high and holds the DEP carbon electrodes. The other channel is 1 mm wide and 100 μm high and is used for sample retrieval. After manual alignment of the flow channel to the 3D DEP carbon electrodes, the fluid network is sealed against the substrate holding the carbon DEP electrodes. The cross section of a carbon-DEP chip when containing 70 μm high electrodes is illustrated in Fig. 1 (b). The percentage of channel height covered by carbon electrodes is 40% and 70% with the use of 40 and 70 μm high electrodes respectively. The interface of the signal generator to the carbon-DEP chip was detailed above.

Materials and Methods

Experimental sample

Yeast culture is obtained by dissolving 200 mg of yeast cells (*S. cerevisiae*, Sigma-Aldrich) in 10 ml sterile YPD (for yeast peptone dextrose) broth (MP Biomedicals) and incubating the culture aerobically at 30°C with 150 RPM rotation for 18 hours. This culture is then diluted into 100 ml of YPD broth and incubated as before for a further 24 hours.

8 μm latex beads are purchased from Duke Scientific (now part of Thermo Fisher Scientific) and used as received.

The experimental sample consists of a mixture of 8 μm latex particles and yeast cells suspended in a DI water-based 0.1% Bovine Serum Albumin (BSA) solution (Albumin Bovine Serum, Sigma Aldrich) and features a pH of 4.4 (Oakton pH meter, pH2100 Series), a conductivity (σ) of 31.2 μS cm⁻¹ (Oakton conductivity meter, CON510 Series) and a particle concentration of 2.75 X 10⁵ particles ml⁻¹ with 60% latex and 40% yeast cells.

DEP

The dielectric characterization of the experimental sample is performed using Mathematica 5.2 for students (Wolfram Research Inc., Champaign, IL). Yeast cells, both viable and non viable, are modeled as two-shell particles using the dielectric parameters derived by Huang, et al⁶⁵ and following the approach described in the same reference. Modeling of the latex particle is carried out following the work by Morgan and colleagues^{66, 67} and accepting a surface conductance, K_s , of 1.3 nS based on the particle diameter of 8 μm⁶⁶.

Experimental

Experiments are performed using either 40 or 70 μm high carbon electrode posts. A sinusoidal signal with frequency 200 kHz and amplitude of 20 V_{pp} is used to selectively filter yeast cells, viable and non viable, from latex particles. In agreement with our DEP models (Fig. 1 under Electronic Supplementary Information[†]), a working frequency of 200 kHz is optimal to induce the strongest positive DEP force on both non viable and viable yeast cells and attract them to the nearest electrode surface. At that same frequency, the latex

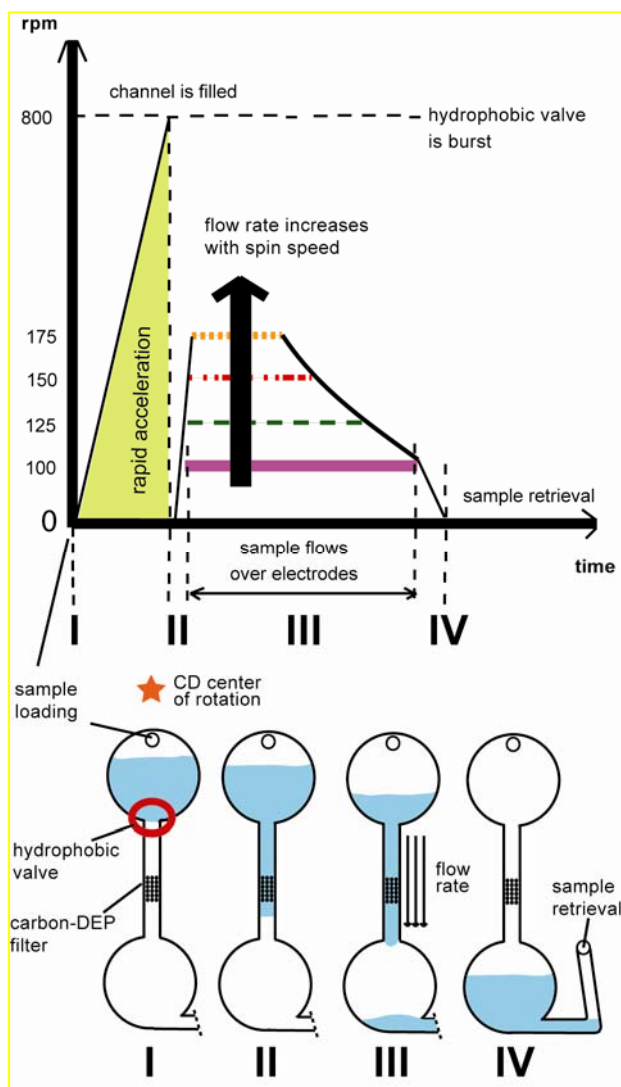


Figure 2 Experiment timeline (top) and corresponding processing steps (bottom): I. sample is loaded in the chamber; II. hydrophobic valve is burst and channel is filled; III. sample flows over carbon-DEP filter at a desired flow rate and IV. sample is retrieved

particles are repelled from the nearest electrode surface by a negative DEP force and are eluted by the fluid flow. At working frequencies higher than 200 kHz, the force exerted on viable yeast increases but that on the non viable yeast cells diminishes. At frequencies lower than the optimal frequency of 200 kHz, the DEP force on non viable yeast cells remains the same as that at 200 kHz but the force acting on viable yeast cells decreases.

The experimental protocol detailed next is illustrated in Fig. 2. A volume of 50 μl of the experimental sample is first introduced into the inner chamber (the chamber closest to the CD center of rotation) where it is prevented from flowing into the channel containing the electrodes during loading by the hydrophobic valve in the inner chamber-channel interface²⁵. Upon sample loading, the carbon electrodes are polarized using the sinusoidal signal detailed above. The channel containing the electrodes is then filled with the sample solution by rapid acceleration of the CD up to 800 rpm which causes the hydrophobic valve to burst²⁵. Once the channel is

filled, the platform is set to spin at a constant speed to induce a desired flow rate (which increases proportional to the spin speed). After the whole volume has passed through the channel the platform is stopped and the sample is retrieved from the outer chamber (the chamber closest to the CD outer edge) via the 1 mm wide channel. Electrodes are de-polarized after sample retrieval.

Sample flow rates are calculated by dividing the volume of the sample that flows from the inner to the outer chamber by the time it takes to do so. This time was assessed visually using the stroboscopic video microscopy system detailed above. Experimental times range from 1 to 16 min. Particle sedimentation becomes an issue with long experiment times (>5 min) and is further addressed below under Impact of particle sedimentation on filter efficiency.

Particle counts used in the quantification of filter efficiency (detailed in the next section) are carried out visually at a 200X magnification using a Nikon Eclipse LV100 Microscope. A hemacytometer set (Hausser Scientific) featuring an improved Neubauer ruling is used to aid in the count. The count values used for filter efficiency quantification (for example number of yeast cells in the sample after DEP-assisted filtration or the number of latex particles introduced in the DEP chip) are the average of four different counts performed for each sample. The standard deviation of the data set (each set has four counts) for a given sample was negligible and is not reported. Visual differentiation between latex particles and yeast cells is achieved without the use of any type of staining technique as their morphology is significantly different.

Data analysis

The targeted particles in this work are yeast cells. The efficiency η when filtering a targeted particle from a mixture is defined as the ratio of the number of targeted particles trapped in the filter over the total number of targeted particles upstream of the filter. We name PI the number of targeted particles upstream of the filter. The number of targeted particles trapped in the DEP filter is given by the difference between PI and the number of targeted particles retrieved after the DEP filter which we name PO . Filter efficiency is then quantified as:

$$\eta = \frac{\text{ParticlesTrapped}}{\text{ParticlesUpstream}} = \frac{PI - PO}{PI} \quad (10)$$

To better illustrate the improvement on efficiency achieved with the use of carbon electrodes at different flow rates (details below under Impact of particle sedimentation on filter efficiency) the filter efficiency is normalized by dividing the number of targeted particles introduced in the DEP chip (PI) by the total number of all particles present in the mixture introduced in the chip (denoted by TI). In a similar way, the number of targeted particles retrieved from the chip (PO) is divided by the total number of all particles contained in the sample retrieved from the DEP chip (given by TO). The normalized equation is then:

$$\eta = \frac{\frac{PI}{TI} - \frac{PO}{TO}}{\frac{PI}{TI}} \quad (11)$$

As denoted in both Equations 10 and 11, a filter efficiency of one is achieved when targeted particles are absent in the sample retrieved from the DEP chip ($PO = 0$) while a filter efficiency equal to zero is obtained when all targeted particles introduced in the DEP chip are retrieved from it after the experiment ($PI = PO$).

Results and Discussion

Electrical and mechanical characterization of the experimental setup

Electrical tests demonstrate how 20 V_{pp} sinusoidal signals with frequencies ranging from 1 kHz to 2 MHz are transmitted from the stationary function generator to a stationary measuring oscilloscope via the rotating CD platform without noticeable losses. Signal frequencies higher than 2 MHz cause impedance loading of the measurement circuit and lead to inappropriate readings⁶⁸. The platform is capable of spinning at frequencies up to 7000 rpm (116.6 Hz) without significant vibrations.

Flow rate characterization of the carbon-DEP chip

Filter efficiency in a DEP chip depends on the flow rate implemented in the channel: hydrodynamic forces compete with the DEP trapping force and too high a flow decreases the number of targeted particles than can be trapped (details in the next section). The flow rate induced in different carbon-DEP chips is characterized as a function of the rotation speed of the platform. The surface materials of the micro channels in carbon-DEP chips consist of double-sided pressure sensitive adhesive for the side walls, polycarbonate for the ceiling and SU-8 for the floor. Polycarbonate and SU-8 surfaces are expected to have a surface roughness on the order of hundreds of nanometers but side walls can present roughness on the order of micrometers as observed under the optical microscope (not shown). Such surface roughness has not been observed to be detrimental to the performance of the device. Negative effects such as flow turbulence or undesired cell trapping in wall crevices could not be discerned. The distribution of flow rates in both carbon-DEP chips (featuring either 40 μm high electrodes, as in CHIP 1, or 70 μm high electrodes, as in CHIP 2) when flowing the experimental sample at spin rates ranging from 100 to 175 rpm is shown in Fig. 3 (a). Flow rate in the channel increases with spin speed. Spin rates between 100 and 175 rpm can induce flow rates as low as 2 μl min⁻¹ and as high as 45 μl min⁻¹ when using the channel geometry implemented here. However, spin speeds below 125 and 100 rpm for CHIP 1 and 2 respectively do not induce a flow in the micro channel observable using our specific imaging system (so it is possible that flows of the

order of nl min⁻¹ do occur). Flow rates are relatively consistent at lower spin rates but exhibit a significant variation at 150 and 175 rpm for CHIP 1 and 2 respectively. It was previously suggested⁶⁹ that the cause for the observed variability of the flow rate at a given rpm is due to the crude way of timing the flow (by eye) and this most likely is the case here as well. The variability in flow rates at high speeds (150-175 rpm) is higher than that at low spin speeds (100-125 rpm). For example at a flow rate of 30 μl min⁻¹, timing errors of ±1, ±2 and ±3 s represent a percentage change of 1, 2 and 3% respectively while this only represents a change of 0.1, 0.3 and 0.5% at a flow rate equal to 5 μl min⁻¹ (considering a sample volume of 50 μl in both cases). To improve the flow rate reading one must consider incorporating a flow sensor in the channel. One option is the use of a flow sensor as introduced by Collins and Lee⁷⁰ who rely on the change of electric admittance on a set of parallel gold electrodes positioned at the channel bottom to measure flow rates up to 35 μl min⁻¹. Another example, more suitable for the measurement of low flow rates, is described in the work by Wu and Sansen⁷¹ who measured flow rates between 1 and 15 μl min⁻¹ using the electrochemical time-of-flight of oxygen which was quantified using micro fabricated amperometric sensors. The difference in induced flow rate between the channels of CHIP 1 and 2 at a given rpm observed in Fig. 3 (a) is due to the unintended differences in alignment of each of the channels side-walls to a radial straight line between the center of rotation of the disk and its outer rim. To demonstrate the deleterious effect of this misalignment we characterized it a bit further. Using Equation 6 we compare the induced flow rate in a channel that is perfectly aligned to the mentioned radial line with the flow rate in channels with different kinds of misalignments to that same radial line. As shown in Figure 3(b) the misalignment is represented by variations in r_1 and/or r_2 . Here r_1 and r_2 are respectively the channel start point (or the point of the channel closest to the CD center of rotation), and the channel end point (or the point of the channel furthest away from the center of rotation). The calculated values are shown in Fig. 3 (c) as a function of spin speed and compared to the experimental curves previously shown in Fig. 3 (a). The experimental results fall within the area delimited by misalignment errors of the channel. Furthermore, Fig. 3 (d) shows how different kinds of misalignments impact the induced flow rate. Flow rate at a given spin speed decreases more rapidly when the channel end point is misaligned (case II in Fig. 3 (b)) than when the channel start point is misaligned (case III in Fig. 3 (b)). A misalignment of start and end points (case IV in Fig. 3(b)) leads to a linear decrease in flow rate that reaches zero faster than in both previous cases. The flow rate is zero when r_1 and r_2 are equal, *i. e.*, when the channel is parallel to the center of rotation, as predicted by Equation 5 ($\Delta r = 0$). We are currently working on a standardized fabrication process to minimize undesired misalignments of the channel to the center of rotation when positioning the DEP modules in the CD platform. Further ongoing work includes flow rate characterization of other suspending media used for biological assays.

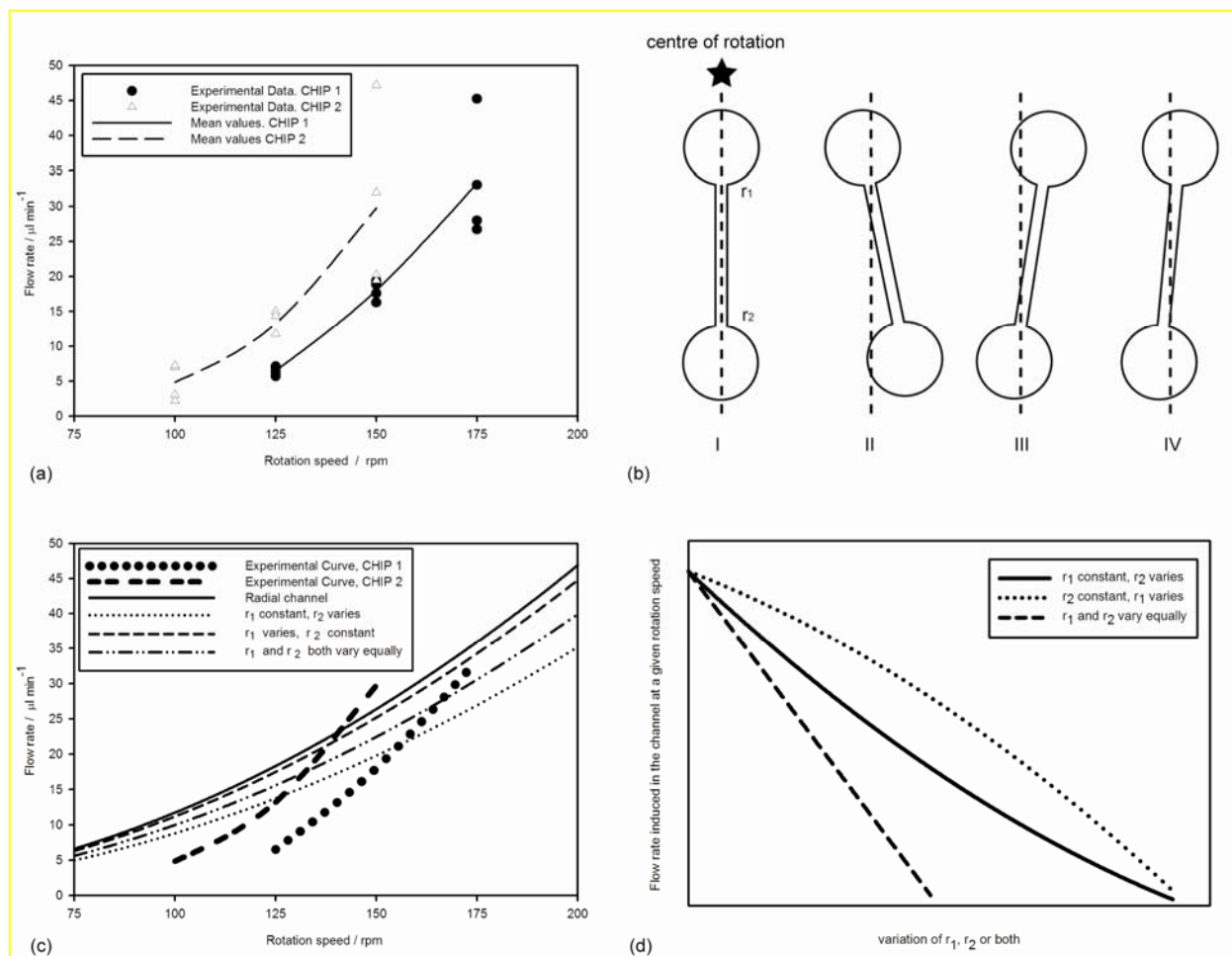


Figure 3 (a) Flow rates established in both carbon-DEP chips at different rotation speeds. CHIP 1 contains 40 μm -high electrodes while CHIP 2 features 70 μm -high electrodes. (b) Different kinds of channel misalignment to a radial line from the centre of rotation to the CD edge. (c) Comparison between the flow rates established in the channel during experiments and those obtained theoretically considering different kinds of misalignments. (d) Impact on the flow rate in the channel as the starting (r_1) and end (r_2) points of the channel vary

Filtering of yeast cells from latex particles

The normalized filter efficiency when filtering yeast cells, from latex particles using either 40 or 70 μm -high carbon electrodes as calculated from Equation 11 is shown in Fig. 4. The red dotted horizontal line denotes a base line given by the average of control values. Control values are obtained in the absence of a polarizing bias on the carbon electrodes. The use of 70 μm high carbon electrodes yields a 100% filter efficiency at flow rates below 5 $\mu\text{l min}^{-1}$ and constitutes a better filter than the one based on 40 μm high electrodes when considering flow rates below 10 $\mu\text{l min}^{-1}$. At flow rates between 10 and 35 $\mu\text{l min}^{-1}$ the situation reverses and the use of 40 μm high electrodes yields a better efficiency. Based on our simulation results we suspect that this result is due to experimental and statistical errors. The use of 70 μm -high electrodes offers more trapping volume and a better coverage of the channel height than the use of 40 μm -high ones at any given medium conductivity and polarizing voltage (Fig. 2 under Electronic Supplementary Information[†]). The improvement of filter efficiency over the control base line approaches zero at flow rates above 35 $\mu\text{l min}^{-1}$. Above this

flow rate the hydrodynamic force overcomes the DEP trapping force. From Equation 11 the filter efficiency must obviously be zero when no particles are trapped by the filter, however in practice, undesirable experimental conditions such as particle sedimentation (see next section), adsorption to the channel surface, physical trapping of particles in crevices present in the micro channel, etc. explain this non-zero value of the control.

Ongoing work focuses on the improvement of the filter efficiency of carbon-DEP designs. The trapping volume of a carbon-DEP filter in a flow channel depends on the surface area of the individual electrodes, the number of electrodes contained in the filter array, the gap between electrodes and the voltage applied to the electrodes. The number of electrodes that can be contained in a given volume of the channel depends on both the volume of the individual electrodes and the gap between them, for example, an array can be very dense when it contains slim tall electrodes separated by narrow gaps. A reduction of the gap width is of particular interest in DEP because it lowers the amount of voltage that must be applied to obtain an electric field with a magnitude suited for DEP manipulation ($\sim 10^5 \text{ V/m}^2$).

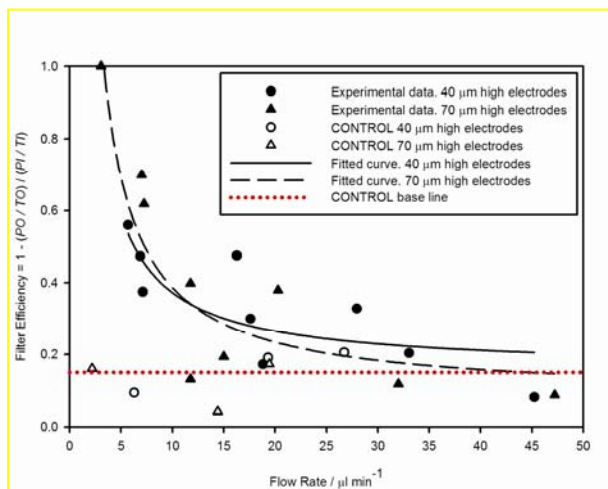


Figure 4 Normalized filter efficiency at different flow rates. Yeast cells are selectively filtered from latex particles using either 40 or 70 μm -high electrodes

However, the gap width must be big enough to be able to accommodate the size of the particles contained in the sample to prevent the electrode array from acting as an unselective physical filter. The use of low voltages to generate a given electrical field relaxes the specifications of a DEP-based platform and makes it more amenable to be used in a practical setting, for example point-of-care applications. In carbon-DEP a voltage loss between the connection pad (used to interface the chip with a function generator) and the base of the electrodes is often introduced. The lower conductivity of carbon compared to that of metals⁴⁸ creates an ohmic loss that is dependent on the shape and the dimension of the carbon structure and must be taken into account. In general, this connection resistance can be reduced by using large connection pads and electrical leads that are wide, thick and short in length. The voltage drop across the height of the carbon electrodes is negligible when their height is below or equal to 100 μm (confirmed by simulation results shown elsewhere⁷³). A detailed optimization process of the carbon-DEP filter is beyond the scope of this work and will be presented elsewhere.

The filter efficiency when working with biological samples benefits from the use of a suspending media with low conductivity and yet capable to support biological particles. For example, RPMI (for Roswell Park Memorial Institute) is a low conductive ($\sigma = 150 \mu\text{S cm}^{-1}$) medium utilizing a bicarbonate buffering system and varying amounts of amino acids and vitamins. This medium has already been demonstrated to be benign and efficient for the DEP manipulation of stem cells¹⁵.

Impact of particle sedimentation on filter efficiency

The filter efficiency as a function of the flow rate in the channel is again shown in Fig. 5 (a) but now as calculated from Equation 10. Dashed and solid lines denote curves fitted to experimental data points (black curves) and control data points (red curves). The improvement of the filter efficiency over the control can be gleaned from Figure 5 (b). Comparing Fig. 5 (a) with Fig. 5 (b) gives us an insight about the impact of particle sedimentation on filter efficiency at different flow

rates. At flow rates below 10 $\mu\text{l min}^{-1}$ the DEP trapping force overcomes the hydrodynamic force and filters most of the yeast cells. Even though the filter efficiency obtained with the use of either 40 and 70 μm high electrodes is close to one at flow rates below 10 $\mu\text{l min}^{-1}$ the improvement over the control experiments carried on at similar flow rates is minimal. Low flow rates translate in slow flow velocities that allow for enough time for latex particles (and yeast cells that are not trapped in the filter) to sediment. Upon sedimentation, latex particles (and yeast cells) are likely to adsorb on the channel surfaces which results in low particle counts in the retrieved sample. At flow rates between 10 and 25 $\mu\text{l min}^{-1}$ the DEP trapping force is still stronger than the hydrodynamic force and filters a high percentage of the total population of yeast cells in the sample but now the flow velocity is fast enough to prevent sedimentation and effectively elutes the latex particles (and the yeast cells that could not be trapped) out of the channel. It is in this range where the highest improvement is achieved as illustrated in Fig. 5 (b). At high flow rates the hydrodynamic force completely overcomes the DEP trapping force exerted on the yeast cells by the electrode array and elutes all particles contained in the sample. In this case the improvement of filter efficiency over the control is minimal as illustrated at flow rates above 35 $\mu\text{l min}^{-1}$ in Fig. 5 (b). A further experimental result to quantify sedimentation comes from the comparison between the number of total particles per unit volume that are retrieved from the chip and those initially introduced in it. At flow rates below 10 $\mu\text{l min}^{-1}$ the number of total particles retrieved from the chip is in average 58% of the total number of particles introduced in it and leads to an estimated 42% loss of particles due to sedimentation. No leaks were discerned in the experimental setup and the possibility of loss of particles from the fluid network is eliminated. Furthermore, at flow rates above 10 $\mu\text{l min}^{-1}$ the number of particles retrieved from the chip is close to the total count of particles introduced into it.

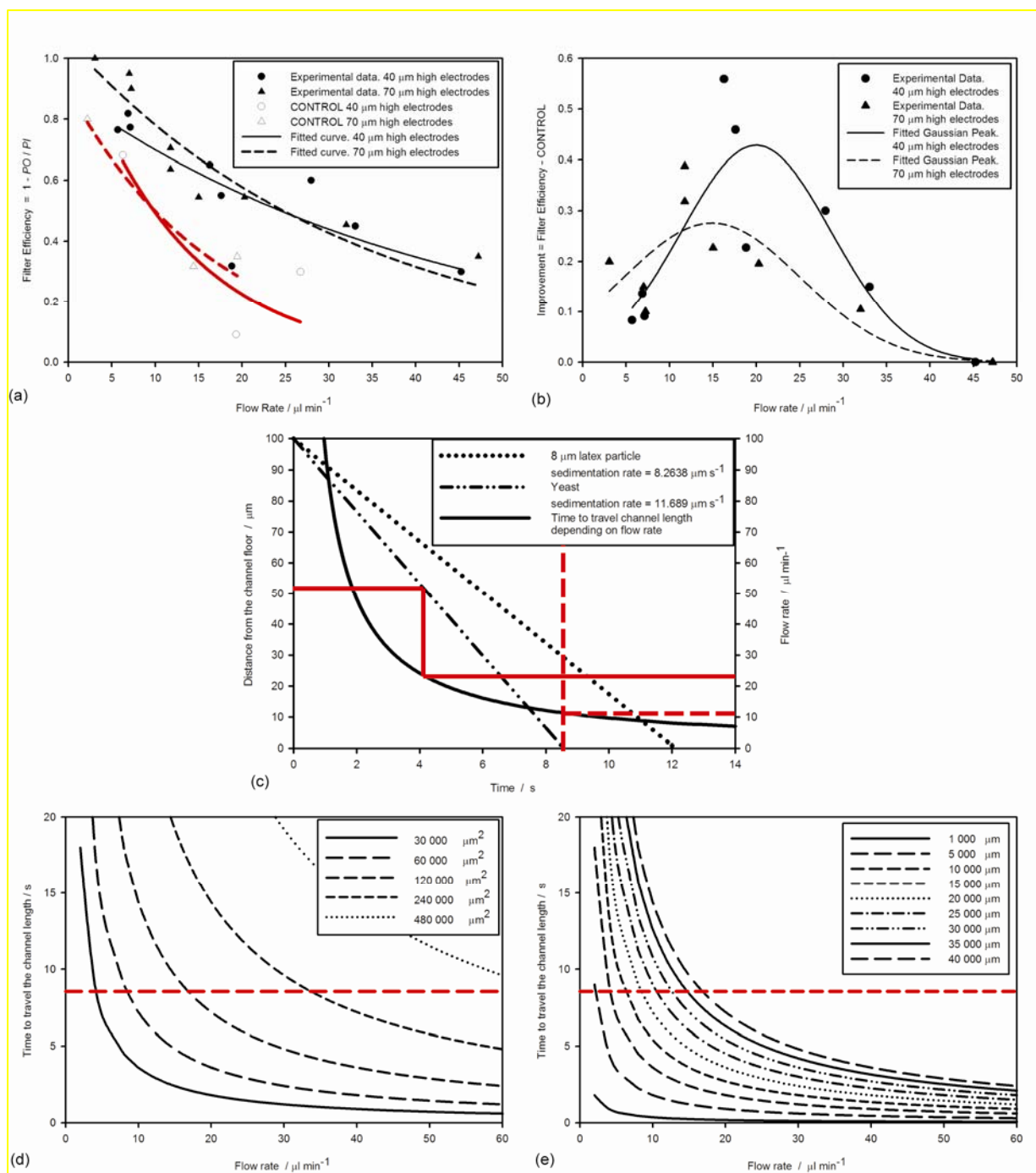
Future designs must account for the sedimentation effects described here. The sedimentation velocity U_s of a spherical particle in a given media can be derived by equating the Stokes drag force of the particle ($D_s = 6\pi\mu r U_s$) with its weight minus buoyancy:

$$6\pi\mu r U_s = \frac{4}{3}\pi r^3 (\rho_{particle} - \rho_{fluid})g \quad (12)$$

solving for U_s yields:

$$U_s = \frac{2r^2 (\rho_{particle} - \rho_{fluid})g}{9\mu} \quad (13)$$

where μ is the viscosity of the media, r is the particle radius, ρ_{fluid} is the density of the media, $\rho_{particle}$ is the density of the particle and g is gravity (equal to 9.81 m s^{-2}). U_s is also known as Stokes velocity and can be used to calculate the maximum time a particle can travel in a channel without sedimenting. Equation 13 describes the sedimentation velocity of an isolated particle immersed in an infinitely dilute solution



and is used here as a basic model for particle sedimentation.

Fig. 5. (a) Filter efficiency at different flow rates when using 40 and 70 μm -high electrodes to filter yeast cells from latex particles. (b) Improvement of filter efficiency over control experiments as flow rate increases. The improvement of filter efficiency at low flow rates is not significant due to particle sedimentation. (c) Sedimentation rate of latex particle and yeast cells (dotted and slash lines) and time it takes for them to travel the channel length depending on the flow rate implemented in the channel (solid curve). Experiment times longer than 8 s (and flow rates less than 11 $\mu\text{l min}^{-1}$) allow for all yeast cells to sediment on the channel bottom (dashed red lines). Experiment times of around 4 s (and flow rates above 20 $\mu\text{l min}^{-1}$) reduce the number of particles settled on the channel floor to those initially positioned on the lower half of the channel (solid red lines). (d) Time to travel the channel length vs. flow rate for channels with fixed cross section area (600 μm by 100 μm) but varying length. The use of shorter channels allows for slower flow rates and avoids particle sediments. (e) Time to travel the channel length vs. flow rate for channels with fixed length (25 000 μm) but varying cross section area.

The use of channels with bigger cross section areas requires faster flow rates to avoid particle sedimentation. Red horizontal dotted lines in (d) and (e) mark the threshold at 8.55 s where all yeast cells contained in a 100 μm -high channel sediment as illustrated in (c).

This idealized condition does not apply for a typical experimental sample where a particle is part of a large

assembly of particles. However, modeling of particle settlement in a dense particle environment requires the use of

computer simulation⁷⁴ and is beyond the scope of the current work. For instance, settling of particles in a dense solution creates velocity perturbations in the surrounding fluid that lead to long-range hydrodynamic interactions between the particles and causes a decrease in their settling velocity as compared to the idealized Stokes velocity.

To prevent particle sedimentation from negatively impacting the DEP filter efficiency a lower limit of the flow rate to be implemented in the channel must be calculated. For example, the analysis based on Fig. 5 (b) identified that flow rates below $10 \mu\text{l min}^{-1}$ are to filter efficiency.

Next we illustrate a method to define an optimal range of flow rate values such that the particles that are not trapped by the filter are effectively eluted out of the channel.

The flow rate Q in the channel equals the product of flow velocity V times channel cross-section A ,

$$Q = VA \quad (14)$$

while the time t for a particle to travel a given channel length equals the ratio of channel length L to flow velocity V ,

$$t = \frac{L}{V} \quad (15)$$

Therefore the time required for a particle to travel a given length L of a channel with cross-section A can be calculated as a function of flow rate as:

$$t = \frac{LA}{Q} \quad (16)$$

by equating flow velocity in Equations 14 and 15. The channel used in this work features a length of 26.84 mm and a cross-section area of $600 \mu\text{m}$ by $100 \mu\text{m}$. The relation between the time for a particle to travel the channel length and the flow rate, based on Equation 16, is illustrated in Fig. 5 (c). The sedimentation rates of yeast cells and latex particles are presented in this figure as well. The sedimentation rate of yeast cells ($11.689 \mu\text{m s}^{-1}$) and latex particles ($8.2638 \mu\text{m s}^{-1}$) is calculated from Equation 13 and is shown for the best case scenario of yeast cells and latex particles flowing close to the ceiling of the channel ($100 \mu\text{m}$ high). In this case, yeast cells may reach the bottom of the channel as fast as in 8.55 s while latex particles can do so in 12 s. The sedimentation rate of a given particle is constant regardless of the initial position of the particle in the channel and particles flowing closer to the channel bottom sediment faster. Fig. 5 (c) helps in the establishment of an optimal flow rate that prevents particle sedimentation. For example, flow rates below $11 \mu\text{l min}^{-1}$ are undesirable since they are too slow and allow for the sedimentation of all yeast cells (red dashed lines). However, the use of higher flow rates decreases the time a particle takes to travel the channel length. For instance, flow rates of around $24 \mu\text{l min}^{-1}$ transport the particles across the channel length in 4 s and during that time only those particles initially at a height of $50 \mu\text{m}$ or less from the channel bottom may sediment (red solid lines). The use of a design aid as represented in Fig. 5

(c) must also take into account the fact that above certain flow rates the filter efficiency significantly drops as illustrated in Fig. 4. If the flow rate desirable to avoid particle sedimentation yields a too low DEP filter efficiency for a given channel, the channel length and cross-section must be adapted to allow for slower flow rates, increased filter efficiency while also avoiding particle sediments. Channels with different lengths and constant cross-section ($600 \mu\text{m}$ by $100 \mu\text{m}$) and with different cross-sections and constant length ($25\ 000 \mu\text{m}$) respectively, are compared in Fig. 5 (d) and (e) in terms of the time it takes for a particle to travel the channel length given a fixed flow rate. The different curves are obtained using Equation 16. In contrast to the use of long channels, implementing shorter channels allows for slower flow rates in the channel and avoids particle sedimentation. For example, an horizontal line at 8.55 s (red dashed line) in Fig. 5 (d) establishes the range of channel lengths (shorter than $15\ 000 \mu\text{m}$) where flow rates below $10 \mu\text{l min}^{-1}$ can be implemented without experiencing yeast sedimentation. However, the use of shorter channels limits the number of electrodes that can be contained in the channel and decreases the trapping volume available in the channel. The impact of increasing channel cross section on the time it takes for a given particle to travel a given channel length of $250\ 00 \mu\text{m}$ as flow rate increases is shown in Fig. 5(e). An increase of channel cross section requires the implementation of faster flow rates to avoid particle sedimentation. For instance, a channel cross section of $100 \mu\text{m}$ high and $1\ 200 \mu\text{m}$ wide ($A = 120\ 000 \mu\text{m}^2$) requires the use of a flow rate as fast as $20 \mu\text{l min}^{-1}$ to avoid sedimentation of a yeast cell flowing at the top of the channel (sedimentation time equals 8.55 s in this case and is denoted by the red dashed line). Unfortunately, at such high flow rate the DEP trapping force is completely voided by the hydrodynamic force and no yeast cells can be trapped. Plots like the ones in Figures 5 (c), (d) and (e) aid the process of reaching a compromise between trapping volume and channel dimensions to avoid particle sedimentation and improve the filter efficiency of a DEP device.

Advantages of the system

The CD-based DEP platform (SpinDEP) demonstrated here offers key advantages compared to more traditional DEP platforms with peristaltic or syringe pumps: 1) Footprint reduction; the current platform has the footprint of a data compact disc and a height less than 5 cm. 2) Cost reduction; external fluidic interconnects such as tubing, sample loading docks/ports, valves, splitters and/or syringe connectors are eliminated. Furthermore, because the flow rates induced in a channel by centrifugal forces (which can be as low as 5 nl/s ⁶⁹) depend mostly on the channel dimensions and its relative position and orientation to the center of rotation, high precision motors as those required in syringe pumps are not needed in centrifugal pumping. 3) Centrifugal pumping is “contact free” and does not require any mechanical interconnects to induce a pressure gradient for pumping. The virtual nature of the pumping force results in a vented system that is immune to the presence of air bubbles. 4) The

demonstrated platform is a self-contained platform which minimizes the probability of sample leakage from the experimental setup. The complete fluidic network (and indeed the experiment or clinical test) can be contained in a single device (which can be disposable), be it a chip that can be embedded in a CD or the whole disk itself. 5) Centrifugal pumping does not depend on the physicochemical properties of the sample. 6) The demonstrated DEP platform is modular and amenable to integration with other sample preparation and detection architectures already demonstrated in CD-based platforms. It is important to clarify that the current platform does not operate at the point-of-care yet. Ongoing work is on the replacement of bulky and complex instrumentation, such as the described visualization system and the motor spins stand, for a miniaturized, less expensive stand-alone system. The motor required for a SpinDEP unit at the point-of-care is expected to be similar to those used in conventional data CD units. The incorporation of flow rate sensors inside the fluid network (described above under Flow rate characterization of the carbon-DEP chip) eliminates the need for a visualization system like the one used in this work. The measurement of a desired variable, for example the concentration of a targeted cell population after enrichment, can be performed on the CD using fluorescence and absorption measurements or electrical methods such as dielectric spectroscopy.

The addition of electrical forces to the CD platform affords a variety of functions previously not possible in CD fluidics: 1) Electrokinetic phenomena such as electrophoresis and dielectrophoresis allow for the bulk manipulation of cells, DNA and proteins with higher selectivity than hydrodynamics and centrifugation. It also allows for the selective manipulation and analysis of single entities, for example the isolation and electroporation of single cells to increase the efficiency in cell transfection for the genetic modification of stem cells⁷⁵. 2) Electrodes in a centrifugal fluidic network enable novel mechanisms for analysis such as dielectric spectroscopy and electrochemical sensors. 3) Electric power on-CD permits the installation of different transducer modules on the CD and can enable the continuous interaction of forces such as optical, thermal and sonic with centripetal and electrical forces. Current CD platforms rely on external stationary transducer modules that only allow for intermittent interaction with a specific area of the CD (although the higher the spin rate the less intermittent the interaction is) and may require the CD to become stationary to acquire data or manipulate a variable. While some applications may not require continuous interaction or even benefit from stationary conditions, real-time sensing of processes with fast kinetics and continuous manipulation of variables and objects of interest can prove beneficial in other applications. 4) The propulsion of fluids in current CD platforms is limited to centrifugal pumping from the center of a disk to its rim. Often this prevents the implementation of a whole diagnostic system in a single CD since cascading of all required functions (sample preparation, sorting, detection, etc.) cannot be fitted in the radius of a standard-sized CD. Electrokinetic phenomena can be used to drive a sample volume towards the CD center after centrifugation. For

example, electroosmotic flow can return fluids to the CD center which gives the user the choice to drive the sample volume through the same processing network or to transfer to adjacent processing steps. 5) Electrical forces scale down favorably and can prove to have a stronger impact than centripetal forces in nanofluidics applications.

Conclusions

The use of centrifugal forces for fluid pumping and fluid manipulation improves traditional DEP platforms in terms of footprint, cost, robustness and practicality. 3D carbon-electrode DEP, or carbon-DEP, offers key advantages over the use of other DEP techniques including a simple and inexpensive fabrication process. The implemented modularity allows for the use of interchangeable disposable chips depending on the type of assay or study to be conducted. Other electrokinetic-based applications besides filtering are targeted including cell, microorganism and biomolecule sorting and cell electroporation for DNA release and transfection.

In this work, we advance the state-of-the-art in CD fluidic platforms by interfacing programmable electrical signals to the rotating disk. The combination of electrical and centrifugal forces in a single platform expands the number of applications where centrifugal microfluidics and electrokinetics are used by themselves. Electrokinetic phenomena does not scale up favorably since the magnitude of an electric field is inversely proportional to the separation between electrodes. Fluid manipulation using CD fluidics and centripetal forces does not scale down favorably since the fluidic resistance of a channel increases exponentially with a decrease in channel cross-section. In view of this, certain assays and fluidic functions may benefit better from electrokinetics than from CD fluidics and *vice versa*. An integrated system like the one demonstrated here is thus desired. For example, a CD-based sample-to-answer system can be engineered where sample preparation (mixing, conjugation, metering, splitting, lysis, etc.) is carried on using centripetal forces while selective fine manipulation is implemented with electrokinetics (electrophoresis, dielectrophoresis, electroporation, etc.). Ongoing work pertains to the integration of electrokinetic capabilities with CD fluidics towards automated platforms for point-of-care diagnostics and cell and bioparticle sorting.

Acknowledgements

The authors thank Dr. David Smith from EXIQON Diagnostics (Tustin, CA) for facilitating yeast cultures.

Notes and references

- ^a Mechanical and Aerospace Engineering Department, University of California, Irvine. 4200 Engineering Gateway, Irvine, CA 92697, USA. E-mail: drmartnz@gmail.com; Tel: +1 949 824 4143
- ^b Biomedical Engineering Department, University of California, Irvine. 3120 Natural Sciences II, Irvine, CA 92697, USA. E-mail: mmadou@uci.edu; Tel: +1 949 824 6585

† Electronic Supplementary Information (ESI) available: [Fig. 1 DEP spectrum of viable yeast cells, non viable yeast cells and latex particles when contained in a medium with conductivity equal to $31.2 \mu\text{S cm}^{-1}$ in the frequency range from 30 kHz to 1 MHz. Fig. 2 Model of the electric field generated around 40 and 70 μm -high electrodes inside a 100 μm -high channel filled with a medium with conductivity equal to $100 \mu\text{S cm}^{-1}$. Electrodes are polarized at 10 V_{pp}] See DOI: 10.1039/b000000x/

§ This carbonaceous material is derived through the pyrolysis of organic polymers such as phenolic resins and furfuryl alcohols^{76, 77}. Although glass-like carbon is similar to vitreous carbon and glassy carbon, the IUPAC (International Union of Pure and Applied Chemistry) suggested the use of the term glass-like carbon over glassy or vitreous carbon as the latter ones have been previously introduced as trademarks⁷⁸.

Ψ The Coriolis force acting on a fluid element in a rotating platform is given by $F_{\text{coriolis}} = 2\rho\omega v$ where v is the velocity of the element moving in/on a rotating platform, ω is the angular velocity of the rotating platform and ρ is the density of the fluid. The Euler force is given by $F_{\text{euler}} = \rho r(d\omega/dt)$. A variation in angular velocity ω of the rotating platform creates an Euler force that is proportional to the density ρ of the fluid and the distance r of the fluid element to the center of rotation.

¶ C-MEMS refers to a fabrication technique where glass-like carbon is obtained through the pyrolysis of organic polymers that have been patterned using photolithography, molding, embossing or any other suitable technique.

1 C. D. Chin, V. Linder and S. K. Sia, *Lab Chip*, 2007, **7**, 41-57.

2 H. Craighead, *Nature*, 2006, **442**, 387-393.

3 P. S. Dittrich and A. Manz, *Nature Reviews Drug Discovery*, 2006, **5**, 210-218.

4 D. Figeys and D. Pinto, *Anal Chem*, 2000, **72**, 330 A-335 A.

5 B. H. Weigl, R. L. Bardell and C. R. Cabrera, *Adv. Drug Deliv. Rev.*, 2003, **55**, 349-377.

6 H. Andersson and A. van den Berg, *Sensors Actuators B: Chem.*, 2003, **92**, 315-325.

7 i-STAT 1
<http://www.abbottpointofcare.com/istat/www/products/analyzers.htm>, 2009.

8 Piccolo xpress <http://www.abaxis.com/medical/piccolo.html>, 2009.

9 H. A. Pohl, *Dielectrophoresis*, Cambridge University Press, Cambridge, 1978.

10 P. R. C. Gascoyne, X. Wang, Y. Huang and F. F. Becker, *IEEE T Ind Appl*, 1997, **33**, 670-678.

11 A. Menachery, S. Chappell, R. J. Errington, D. Morris, P. J. Smith, M. Wiltshire, E. Furon and J. Burt, Proceedings of NSTI Nanotech 2008, Boston, MA, 2008.

12 P. R. C. Gascoyne, X. B. Wang, Y. Huang and F. F. Becker, *IEEE Trans. Ind. Appl.*, 1997, **33**, 670-678.

13 F. F. Becker, X. Wang, Y. Huang, R. Pethig, J. Vykoukal and P. R. C. Gascoyne, *P Natl Acad Sci USA*, 1995, **92**, 860-864.

14 J. Yang, Y. Huang, X. B. Wang, F. F. Becker and P. R. C. Gascoyne, *Anal. Chem.*, 1999, **71**, 911-918.

15 L. A. Flanagan, J. Lu, L. Wang, S. Marchenko, N. L. Jeon, A. P. Lee and E. Monuki, *Stem Cells*, 2008, **26**, 656-665.

16 M. Stephens, M. S. Talary, R. Pethig, A. K. Burnett and K. I. Mills, *Bone Marrow Transplantation*, 1996, **18**, 777-782.

17 Y. Huang, J. Yang, X. Wang, F. F. Becker and P. R. C. Gascoyne, *Journal of Hematotherapy & Stem Cell Research*, 1999, **8**, 481-490.

18 M. S. Talary, K. I. Mills, T. Hoy, A. K. Burnett and R. Pethig, *Medical and Biological Engineering and Computing*, 1995, **33**, 235-237.

19 P. R. C. Gascoyne and J. V. Vykoukal, *Proc IEEE*, 2004, **92**, 22-42.

20 G. Wang, W. Hsu, Chang Y-Z and H. Yang, *Biomed Microdevices*, 2004, **6**, 47-53.

21 *Pat.*, 6749736, June 15.

22 *Pat.*, 6465225, October 15.

23 M. Boettcher, M. Jaeger, L. Riegger, J. Duerée, R. Zengerle and C. Duschl, *Biophysical Reviews and Letters*, 2006, **1**, 443-451.

24 M. Madou and G. J. Kellogg, *Proceedings of SPIE*, 1998, **3259**, 80-93.

25 M. Madou, J. Zoval, G. Jia, J. Kim and N. Kim, *Annu Rev Biomed Eng*, 2006, **8**, 601-628.

26 J. V. Zoval and M. J. Madou, *Proceedings of IEEE*, 2004, **92**, 140-153.

27 Gyrolab Platform
http://www.gyros.com/en/products/gyrolab_platform/index.html, 2009.

28 J. Steigert, M. Grumann, T. Brenner, L. Riegger, J. Harter, R. Zengerle and J. Ducree, *Lab Chip*, 2006, **6**, 1040-1044.

29 C. T. Schembri, T. L. Burd, A. R. Kopf-Sill, L. R. Shea and B. Braynin, *J. AUTOM. CHEM.*, 1995, **17**, 99-104.

30 B. S. Lee, J. Lee, J. Park, J. Lee, S. Kim, Y. Cho and C. Ko, *Lab Chip*, 2009, **9**, 1548-1555.

31 H. Kido, M. Micic, D. Smith, J. Zoval, J. Norton and M. Madou, *Colloids and Surfaces B: Biointerfaces*, 2007, **58**, 44-51.

32 G. J. Kellogg, T. E. Arnold, B. L. Carvalho, D. C. Duffy and N. F. Sheppard, Proc. of MicroTAS 2000, Enschede, The Netherlands, 2000.

33 G. Martensson, M. Skote, M. Malmqvist, M. Falk, A. Asp, N. Svanvik and A. Johansson, *European Biophysics Journal*, 2006, **35**, 453-458.

34 N. Honda, U. Lindberg, P. Andersson, S. Hoffmann and H. Takei, *Clin. Chem.*, 2005, **51**, 1955-1961.

35 R. Peytavi, F. R. Raymond, D. Gagne, F. J. Picard, G. Jia, J. Zoval, M. Madou, K. Boissinot, M. Boissinot, L. Bissonnette, M. Ouellette and M. G. Bergeron, *Clin. Chem.*, 2005, **51**, 1836-1844.

36 G. Jia, K. Ma, J. Kim, J. V. Zoval, R. Peytavi, M. G. Bergeron and M. J. Madou, *Sensors Actuators B: Chem.*, 2006, **114**, 173-181.

37 H. Chen, L. Wang and P. C. H. Li, *Lab Chip*, 2008, **8**, 826-829.

38 N. Thomas, A. Ocklind, I. Blikstad, M. Griffiths, K. Kenrick, H. Derand, G. Ekstrand, C. Ellström, A. Larsson and P. Andersson, Proc. of MicroTAS 2000, Enschede, The Netherlands, 2000.

39 R. Martinez-Duarte, R. Gorkin, K. Abi-Samra and M. J. Madou, Proceedings of Transducers 2009, Denver, CO, 2009.

40 N. Kim, C. M. Dempsey, C. Kuan, J. V. Zoval, E. O'Rourke, G. Ruvkun, M. J. Madou and J. Y. Sze, *Genetics*, 2007, **177**, 835-845.

41 N. Kim, C. M. Dempsey, J. V. Zoval, J. Sze and M. J. Madou, *Sensors Actuators B: Chem.*, 2007, **122**, 511-518.

42 E. B. Cummings and A. K. Singh, *Anal. Chem.*, 2003, **75**, 4724-4731.

43 B. H. Lapizco-Encinas, B. A. Simmons, E. B. Cummings and Y. Fintschenko, *Anal. Chem.*, 2004, **76**, 1571-1579.

44 B. A. Simmons, G. J. McGraw, R. V. Davalos, G. J. Fiechtner, Y. Fintschenko and E. B. Cummings, *MRS Bulletin*, 2006, **31**, 120-124.

45 R. V. Davalos, G. J. McGraw, T. I. Wallow, A. M. Morales, K. L. Krafcik, E. B. Cummings and B. A. Simmons, *Analytical and Bioanalytical Chemistry*, 2008, **390**, 847-855.

46 C. Wang, G. Jia, L. H. Taherabadi and M. J. Madou, *J Microelectromech S*, 2005, **14**, 348-358.

47 T. Shigemitsu and G. Matsumoto, *Med & Biol Eng & Comput*, 1979, **17**, 470.

48 B. Y. Park, L. Taherabadi, C. Wang, J. Zoval and M. J. Madou, *J Electrochem Soc*, 2005, **152**, J136-J143.

49 G. Turon Teixidor, R. A. Gorkin III, P. P. Tripathi, G. S. Bisht, M. Kulkarni, T. K. Maiti, T. K. Battacharyya, J. R. Subramaniam, A. Sharma, B. Y. Park and M. Madou, *Biomed Mater*, 2008, **3**, 034116.

50 J. Benson, *J Biomed Mat Res*, 1971, **5**, 41-47.

51 S. Yamada and H. Sato, *Nature*, 1962, **193**, 261-262.

52 F. C. Cowlard and J. C. Lewis, *J Mat Sci*, 1967, **2**, 507-512.

53 W. V. Kotlensky and H. E. Martens, *Nature*, 1965, **206**, 1246-1247.

54 G. M. Jenkins and K. Kawamura, *Nature*, 1971, **231**, 175-176.

55 C. Wang and M. Madou, *Biosens and Bioelectron*, 2005, **20**, 2181-2187.

56 R. Martinez-Duarte, S. Cito, E. Collado-Arredondo, S. O. Martinez and M. J. Madou, *Sensors and Transducers Journal*, 2008, **3**, 25-36.

57 B. Y. Park, R. Zaouk and M. Madou, Proceedings of SPIE, 2004.

58 *Pat.*, US 2006/0260944A1, Nov. 23, 2006.

59 B. Y. Park, A. Paradiso, M. Kawabe and M. J. Madou, Proceedings of SPIE, 2006.

60 R. Martinez-Duarte, S. Cito, E. Collado-Arredondo, S. O. Martinez and M. Madou, Proceedings of NSTI Nanotech 2008, Boston, MA, 2008.

-
- 61 R. Martinez-Duarte, J. Andrade-Roman, S. O. Martinez and M. J. Madou, Proceedings of NSTI Nanotech 2008, Boston, MA, 2008.
- 62 R. Martinez-Duarte, H. A. Rouabah, N. G. Green, M. Madou and H. Morgan, Proceedings of MicroTAS 2007, Paris, France, 2007.
- 5 63 B. Y. Park and M. J. Madou, *Electrophoresis*, 2005, **26**, 3745-3757.
- 64 D. J. Beebe, G. A. Mensing and G. Walker M., *Annu Rev Biomed Eng*, 2002, **4**, 261-286.
- 65 Y. Huang, R. Holzel, R. Pethig and X. Wang, *Phys Med Biol*, 1992, **37**, 1499-1517.
- 10 66 N. G. Green and H. Morgan, *J Phys D: Appl Phys*, 1997, **30**, 2626-2633.
- 67 I. Ermolina and H. Morgan, *J Colloid Interf Sci*, 2005, **285**, 419-428.
- 68 S. A. Dyer, *Wiley Survey of Instrumentation and Measurement*, Wiley-IEEE Press, New York, 2001.
- 15 69 D. C. Duffy, H. L. Gillis, J. Lin, N. F. Sheppard Jr. and G. J. Kellogg, *Anal Chem*, 1999, **71**, 4669-4678.
- 70 J. Collins and A. P. Lee, *Lab Chip*, 2004, **4**, 7-10.
- 71 J. Wu and W. Sansen, *Sensors and Actuators A: Physical*, 2002, **97-98**, 68-74.
- 20 72 P. Gascoyne and J. Vykoukal, *Proceedings of IEEE*, 2004, **92**, 22-42.
- 73 R. B. Zaouk, Ph.D. in Mechanical and Aerospace Engineering, University of California, Irvine, 2008.
- 74 E. Guazzelli, *C. R. Mecanique*, 2006, **334**, 539-544.
- 75 A. Valero, J. N. Post, J. W. van Nieuwkastele, P. M. Ter Braak, W. Kruijjer and A. van den Berg, *Lab Chip*, 2008, **8**, 62-67.
- 25 76 E. Fitzer, K. Mueller and W. Schaefer, in *Chemistry and Physics of Carbon*, ed. ed. P. L. Walker Jr., Marcel Dekker, Inc., New York, 1971, pp.238-383.
- 77 E. Fitzer, W. Schaefer and S. Yamada, *Carbon*, 1969, **7**, 643.
- 30 78 E. Fitzer, K. H. Kochling, H. P. Boehm and H. Marsh, *Pure Appl Chem*, 1995, **67**, 473-506.